



Efficiency of dye adsorption by biochars produced from residues of two rice varieties, Japanese *Koshihikari* and Vietnamese *IR50404*

D.T.M. Phuong^{a,†}, N.X. Loc^{a,*†}, T. Miyanishi^b

^aCollege of the Environment and Natural Resources, Can Tho University, Can Tho, Viet Nam, Phone +84-9191-888-34, Fax +84-71-038-31068, email: dtmphuong@ctu.edu.vn (D.T.M. Phuong), Phone +84-91-888-9024, Fax +84-71-038-31068, email: nxloc@ctu.edu.vn (N.X. Loc)

^bGraduate School of Fisheries and Environmental Sciences, Nagasaki University, Nagasaki, Japan, Phone +81-90-448-75412, Fax +81-95-843-2182, email: miyanishi@nagasaki-u.ac.jp (T. Miyanishi)

Received 29 December 2018; Accepted 5 June 2019

ABSTRACT

Adsorption of Methylene Blue (MB) and Bromocresol Green (BG) were examined by using biochars produced from rice residues, straw and husk of Japanese *Koshihikari* and Vietnamese *IR50404* rice varieties, to evaluate their capacity to adsorb dyes and possible adsorption mechanism. Cationic MB dye was more effectively adsorbed than anionic BG dye by all biochars examined. Vietnamese *IR50404* biochars showed higher capacity of adsorption of two dyes than Japanese *Koshihikari* biochars, approximately about 1.5 times for MB and 1.7 times for BG. In varying pH from 2 to 10, alkaline condition increased adsorption of cationic MB dye - approximately by 27.7–33.5% for rice straw biochars and by 86.2–92.2% for rice husk biochars; albeit a slight decrease in adsorption of anionic BG dye by 27.2–32.9% for rice straw biochars and by 47–70.6% for rice husk biochars. The pH experimental results indicated the existence of negative charges in the biochars and their electrostatic interaction with dyes. The adsorption kinetic study supported intra-particle diffusion of dyes, proceeding via a complex mechanism consisting of both surface adsorption and intra-particle transport within the pores of biochars. Thermodynamic analysis of adsorption suggested that the process was spontaneous with negative ΔG^0 values and endothermic with positive ΔH^0 values ($\Delta G^0 = 35.27\text{--}41.94$ kJ/mol; $\Delta H^0 = 3.92\text{--}23.69$ kJ/mol). This paper discussed possible explanation of dye adsorption with physisorption through porous diffusion, hydrogen bonding, $\pi\text{-}\pi$ interaction or $\pi^+\text{-}\pi$ interaction, common to both anionic and cationic dyes, with additional electrostatic interaction for cationic dyes with biochars in aqueous solution.

Keywords: Biochar; Adsorption; Rice straw; Rice husk; Methylene Blue; Bromocresol Green

1. Introduction

Synthetic dyes belong to important class of organic compounds with multiple aromatic rings. Methylene blue (MB), a common organic cationic dye, has been used in various industries. During its use, high quantity of MB goes with wastewater to the water bodies. The presence of MB in water system can be visible at concentrations as low as 1 ppm [1]. Bromocresol green (BG), an anionic dye, also can induce serious environmental problems. The presence of

MB and BG dyes in water bodies can decrease light penetration into the water, hence reduce photosynthesis and make hazardous for the aquatic lives [2]. They are also found to be very harmful in case of ingestion; dangerous in case of skin and eye contact (irritant), and of inhalation [3]. Therefore, elimination of these dyes is important aspects of wastewater treatment before discharge.

A number of physical, chemical and biological methods have been used to remove dyes from wastewater, in which adsorption method has been evaluated as one of the best treatment methods for dye-containing effluent [4]. Adsorption is defined as the accumulation or concentration

*Corresponding author.

†These authors contributed equally to this work.

of substances at a surface or interface, and it is an important phenomenon in most natural physical, biological, and chemical processes [5]. Adsorption in aqueous phase is a complex process involving physical adsorption and chemical adsorption. In the case of physical adsorption, the adsorbate is bound to the surface by relatively weak van der Waals forces and there is no net transfer of electrons from the interacting species. In contrast to physical adsorption, chemisorption involves exchange or sharing or transferring of electrons between the adsorbate molecules and the surface of the adsorbent to form a chemical bond which is much stronger than in the physisorption, for example via π - π bonding [5].

It is the fact that activated carbon is the most widely used adsorbent material in dye wastewater treatment. To date, a variety of alternative adsorbents has been synthesized and proposed for the adsorption of dye pollutants, including aluminas [6], zeolites [7], clays [8], and novel adsorbents such as nanomaterials [9], graphene-based adsorbents [10], magnetic materials [11], and others. In spite of the availability of these various commercial adsorbents, their widespread use is often constrained, mainly because of high cost and limited accessibility [12,13]. Therefore, the high number of studies performed on the adsorption of dye pollutants use low-cost yet efficient adsorbents, such as biochar. In terms of capital cost involved, while activated carbon is basically a form of oxygen-treated char under high production temperatures, biochar is not oxygen treated and requires relatively lower temperatures hence reduces energy and infrastructural requirements [5]. The cost of different biochar production is calculated in a range of \$0.2–0.5 kg⁻¹, whereas adsorbents such as activated carbon cost in a range of \$5–9 kg⁻¹ [14]. Hence, biochar can be an impressive cost-effective pollutant adsorbent compared to activated carbon and other adsorbents [13,15,16].

Biochar has attracted researcher attention due to its impressive adsorptive properties for various dye contaminants. This is attributed to: (1) its high surface area, which assures a high amount of adsorption sites for dye molecules; and (2) the presence of several functional groups on the surface, which can form complexes with many classes of dyes [17]. The sorption capacities and interaction mechanisms of biochar with dye pollutants mainly depend on dye properties/ion charges, biochar chemical composition, biochar properties, modification/activation, aging process, and environmental conditions [18]. The critical environmental factors affecting the overall adsorption efficiency of the biochar include pyrolysis temperature, solution pH, dosage of biochar, contact time, and co-existed ions [19]. Potentially different biochar–dye interaction mechanisms were proposed, mostly π - π -electron donor–acceptor interaction, electrostatic attraction/repulsion, hydrogen bonding, and pore-filling [19,20].

In the literature, many adsorbents have been applied for the removal of MB, for example, activated carbon produced from Peanut shell [21], *Ficus racemosa* plant barks [22], cotton stalks [23], or from rice straw and rice husk [24]. Biochars produced from kenaf fibre [25], Eucalyptus bark [26], sheep manure, pig manure or rabbit faeces [27], modified rice husk [28] and rice straw [29] have also been used for MB adsorption. Adsorption studies conducted for BG removal showed a limited number, involving *Ziziphys num-*

mularia [30], cotton stalks [23], activated *Phragmites karka* [31], or poly(2-phenoxy ethyl [bis(2-hydroxy ethyl)amino] acetate) [32].

The usage of biochar produced from rice straw and rice husk for the removal of MB dye has recently attracted the attention of several researchers. It is because, rice straw and rice husk are insoluble in water, have good chemical stability, high mechanical strength and possess a granular structure. These characteristics make them to be good adsorbent materials for treating dyes from wastewater [33]. Ahiduzzaman and Islam [34] compared the adsorption of MB onto raw rice husk, rice husk biochar and rice husk activated carbon. In their study, biochar was produced by removing the silica from raw rice husk using sodium hydroxide and applying heat at temperature of 600, 700 and 800°C, and activated carbon was produced by using chemical activation with zinc chloride under high temperature of 600, 700, 800 and 900°C. The surface area of samples at 800°C were found to be 28, 331 and 645 m²/g for raw rice husk, biochar and activated carbon, respectively. The MB numbers were found to be 12, 135 and 262 mg/g, respectively [34]. Kindala et al. [35] studied the removal of Methylene Blue (MB) and Bromocresol Green (BG) by *Bryophyllum pinnatum* (Lam.) Kurz stem powder (BPP), its activated carbon (ACBP), and commercial activated carbon (CAC). The maximum monolayer adsorptions capacities of these adsorbents were as follow: On ACBP: 255.754 (pH 11.15) for MB and 195.313 mg/g (pH 3.25) for BG; On CAC: 176.367 (pH 11.15) for MB and 108.342 mg/g (pH 3.25) for BG; on BPP: 61.013 mg/g (pH 11.15) for MB and 51.733 mg/g (pH 3.25) for BG [35].

In this study, the two major types of rice residues, straw and husk of *Koshihikari* and *IR50404* varieties, were chosen to produce biochar adsorbents because of their available in large quantities, inexpensive, require little processing, and are effective adsorbent materials but have not yet been systematically studied. MB has a special affinity for negatively charged surfaces, and its concentration is easily quantified by spectrophotometry. Therefore, MB was chosen as a model compound for removing cationic dyes from aqueous solution in this study. Its strong adsorption onto rice straw or rice husk materials in some studies were reported [28,29,36]. However, little work has been carried out to BG dye adsorption and none has assessed the BG dye using biochars from rice residues. BG dye thus was selected as the model anionic dye for this study.

This is the first paper to study dye adsorption capacity of biochar adsorbents from rice residue varieties in the two famous rice producing countries, Japan and Vietnam. Following the results obtained from physicochemical properties analysis [37], this study investigated the efficiency of biochars for the adsorption of cationic MB and anionic BG dyes in aqueous solution. This study aims to investigate the adsorption capacity between two rice variety biochars and to explore the interaction mechanisms governing dye-biochar adsorption process by using batch adsorption experiment. Effects of various operation conditions (i.e. biochar pyrolysis temperature, solution pH, biochar dosage, initial dye concentration and contact time) had been extensively studied. The interaction mechanisms were explored based on the results of adsorption kinetic, isotherm and thermodynamic studies.

2. Materials and methods

2.1. Preparation and characterization of biochar adsorbent

Biochar preparation and characteristics were described and reported in the previous work of the authors [37]. Following pyrolyzing, the dried biochar samples were ground and sieved into desirable particles (<0.075 mm). Approximately 13.5 g of biochar were rinsed with 500 mL 0.1 M HCl solution at constant stirring for 1 h to enhance adsorption capacity of biochar [38]. Then deionized water was used to wash the biochar several times until the pH of the solution was between 6.0 and 7.0. The biochar was finally dried overnight at 80°C, sieved, and stored in tightly closed glass bottles until used for further adsorption experiments.

pH point of zero charge (pH_{pzc}) of biochars were performed following a previously published procedure [39]. Briefly, CaCl_2 solution (0.005 M) was boiled to remove CO_2 and was cooled down to room temperature, then was adjusted pH with 0.1 M NaOH or 0.1 M HCl if necessary. Biochar (0.06 g) then was added to 20 mL of the pH-adjusted solution, and the solution was shaken for 24 h. The final pH of the solution after 24 h was recorded, then the difference between initial and final pH (ΔpH) was plotted against initial pH values.

In this paper, biochars derived from Japanese *Koshihikari* and Vietnamese *IR50404* rice straw and rice husk were named according to pyrolysis temperature, i.e., JRS300–JRS700, VRS300–VRS700, JRH300–JRH700 and VRH300–VRH700, respectively.

2.2. Dye adsorbate and batch adsorption experiments

2.2.1. Preparation of dye solutions

Methylene Blue (MB) and Bromocresol Green (BG) were chosen for adsorbing by biochars. All the chemicals were purchased from Sigma-Aldrich and were used without any pre-treatment. The stock solution of MB and BG were prepared (1,000 mg/L), and then initial concentrations were adjusted to desired concentration to be used in the batch adsorption experiments, by diluting the stock solution with deionized water. Table 1 provides information about the chemical structure and properties of studied dyes.

2.2.2. Batch adsorption experiments

All the experiments in this study were conducted in triplicates and the average values were reported with standard deviation. Preliminary tests were firstly conducted to determine the optimum experimental parameters such as biochar pyrolysis temperature (300, 500, and 700°C), solution pH (2–10, which was controlled by adding 0.1 M HCl and 0.1 M NaOH), biochar dosage (0.01–0.05 g), initial dye concentration (10–200 mg/L) and contact time (1–720 min). Adsorption experiments were carried out in a 15 mL conical centrifuge tubes containing 10 mL dye solution with initial concentrations of 50 mg/L. Sample tubes were shaken on a shaker (Bioshaker BR-23FH) and operated at 200 rpm. The suspension was centrifuged at 3000 rpm for 10 min and then was filtered through the Whatman filter paper. The filtrates were measured by UV-visible Recording spectrophotometer (Shimadzu UV-2100), at maximum absorbance of the dyes (see Table 1). To obtain the absorbance-concentration profiles of the dyes, calibration curve was plotted between absorbance and concentration of the dye.

The amount of dye adsorbed on per weight of biochar at equilibrium, q_e (mg/g), and the removal efficiency of dye, S (%) are calculated according to Eqs. (1) and (2):

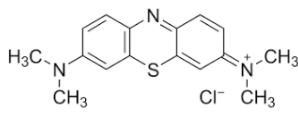
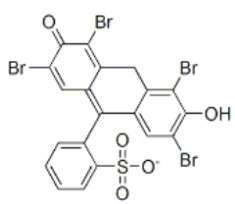
$$q_e = \frac{C_0 - C_e}{m} V \quad (1)$$

$$S = \frac{C_0 - C_e}{C_0} 100 \quad (2)$$

where V (L) is the volume of dye solution; m (g) is the weight of biochar; C_0 and C_e (mg/L) are the initial dye concentrations and dye concentrations at equilibrium, respectively.

The optimum results obtained from preliminary tests were used for kinetic, isotherm and thermodynamic studies. Three different kinetic models, i.e., pseudo-second order, Elovich and intraparticle diffusion model were used. Their nonlinearized forms are included in Supplementary Material Table SM1. The adsorption equilibrium used the non-linear forms of three well-known isothermal models, namely Langmuir, Freundlich and Temkin; their equations are included in Supplementary Material Table SM2.

Table 1
Chemical structure and properties of dyes used in this study

Dyes	Chemical structure	Classification	MW (g/mol)	pK_a	λ_{max} (nm)
Methylene Blue (MB)		Cationic thiazine dye	319.85	3.8	665 (pH neutral)
Bromocresol Green (BG)		Anionic sulfonephthaleins dye	698	4.7	443 (pH acid)

Detailed descriptions of methods and calculations are available in Supplementary Methods.

2.2.3. Error analysis

To find the most suitable isotherm and kinetic models, two different error functions, including chi-square (χ^2) and the coefficient of determination (R^2), were employed. In each case, the parameters were determined by minimizing the respective error functions using the Solver add-in Excel. Below are the calculated expressions of the error functions used.

$$\chi^2 = \sum_{i=1}^n \frac{(q_{e,exp} - q_{e,cal})^2}{q_{e,cal}}$$

$$R^2 = \frac{q_{e,exp} - \bar{q}_{e,cal}}{\sum_{i=1}^n (q_{e,exp} - \bar{q}_{e,cal})^2 + (q_{e,exp} - q_{e,cal})^2}$$

where n : the number of data points; $q_{e,exp}$: the experimental adsorption capacity (mg/g); $q_{e,cal}$: calculated adsorption capacity (mg/g); $\bar{q}_{e,cal}$: average calculated adsorption capacity (mg/g).

3. Results and discussion

3.1. Characterisation of biochars

The details regarding the morphological and chemical characterization of the two rice variety biochars were provided in a previously published paper [37] and were summarized in Table SM3 Supplementary Material. Physicochemical characteristics of biochars that effect the adsorption behaviour of biochar include specific surface area, porosity, surface charge, functional groups, aromaticity and polarity. A brief discussion on these properties is given to evaluate the biochar-dye interaction during the adsorption process.

3.3.1. Specific surface area and porosity

Specific surface area and porosity are often the most important physical properties that influence the adsorption capacity of biochars. Cellulose, hemicellulose, lignin, starch, etc. are thermally broken during pyrolysis of biomass and micropores are formed in biochar due to the loss of water in the dehydration process. Pores formed via this process are highly variable in size and may range from nano- to micrometres in diameter. Biochars are characterized by the presence of micropores (less than 2 nm), mesopores (between 2–50 nm), and macropores (above 50 nm). Pore size is important for dye pollutant because biochar with small pore size cannot capture large dye size [13].

However, it is argued that micropores and small mesopores (2–20 nm) constitute the bulk to the biochar surface area and therefore play a significant role in the sequestration of dyes [40]. Our previous results found that micropores and small mesopores (2–20 nm) occupied over 85% to the total surface area in all biochars. By using intra-particle dif-

fusion kinetic model in this study, it found that pore-filling is a predominant adsorption mechanism of dye molecules onto studied biochars (will be discussed later). According to Hao et al. (2013) and Kasozi et al. (2010), pore-filling effects are mainly controlled by the total micropore and mesopore volumes of the biochar adsorbents especially at low dye concentrations [41,42]. Scanning electron micrograph of biochars, as presented in the previous paper, exhibits a high number of pores and there is a good possibility for the dye molecules to be trapped and adsorbed into these pores.

3.3.2. Surface charge and functional groups

Surface charge and functional groups are among the most important properties for adsorption of dyes. As biochars are applied in an aqueous media for remediation of dye, its surface charge is strongly influenced by the pH of the solution. FTIR analysis in the previous research shows that studied biochars possess various surface functional groups, including carboxylates, carbonyls and hydroxyl groups among others. These functional groups are influenced by the solution pH. The solution pH therefore affects the adsorbent surface charge and controls the adsorption process. The pH at which the surface charge is electrically neutral is known as the point of zero charge (pH_{pzc}). Below the pH_{pzc} , the surface charge of the biochar is positively charged, which would only promote adsorption of cationic dyes while inhibit the uptake of anionic ones; whereas at pH above pH_{pzc} , the surface becomes negatively charged and promotes adsorption of anionic dye [13].

3.3.3. Aromaticity and polarity

The aromatic and polarity properties of biochar are very important for the removal of dye pollutants as these properties promote π - π electron donor interaction, electrophilic interaction, and hydrogen bonding [13]. At high pyrolysis temperature (>500°C), removal of C, H, O elements into gases and other volatile compounds results in changing O/C and H/C ratios in biochar [43]. The O/C and H/C ratios in biochar correlate directly with aromaticity and polarity, which greatly affect its physicochemical properties and thus the dye removal capability [13]. As reported, biochars produced at higher temperature exhibit lower H/C and O/C ratios than that at a lower temperature, indicating a gradual increase in aromaticity and decrease in polarity, with increasing temperature [37]. As a result, rice residue derived biochars produced at 700°C can obtain the higher percent removal compared to those produced at 300 and 500°C.

3.4. Effect of pyrolysis temperature

Biochars produced at 300, 500 and 700°C were chosen for evaluation of the effect of pyrolysis temperature on the adsorption capacity of MB and BG. As mentioned previously, biochar surface area and porosity may strongly influence the adsorption capacity of biochars. In general, elevated temperature pyrolysis generally generates larger pore size and eventually greater surface area, thereby greater adsorption capability. The previous results showed that the val-

ues of surface area and porosity generally increased from 300 to 700°C, where Vietnamese rice variety showed higher surface area and porosity values than Japanese rice variety (VRS > JRS, VRH > JRH); rice straw derived biochars showed higher values than biochars produced from rice husk. In particular, for a gradual temperature increase from 300 to 700°C, the porosity of studied biochars increased from 0.051–0.064 to 0.171–0.299 cm³/g for rice straw biochars, from 0.033–0.045 to 0.164–0.188 cm³/g for rice husk biochars. This was accompanied by an increase in surface area from 23.45–25.89 to 293–378 m²/g for rice straw biochars, from 19.50–25.89 to 235.69–245.05 m²/g for rice husk biochars (see Table SM3 Supplementary Material) [37]. As a result, the removal of dyes increased significantly when the pyrolysis temperature increased from 300 to 700°C (Fig. 1). In particular, the percent removal of MB dye increased from 71.6–72% to 96–99.4% for rice straw biochars, and from 57.6–60.7% to 79.9–82.6% for rice husk biochars. Showing the similar trends, the percent removal of BG dye increased from 46.8–48.2% to 80.2–92.3% for rice straw biochars, and from 29.5–30.5% to 48–49.3% for rice husk biochars. It is therefore concluded that the enrichment of specific surface area by high pyrolysis temperature at 700°C attributed to the rising of biochar removal efficiency. In other words,

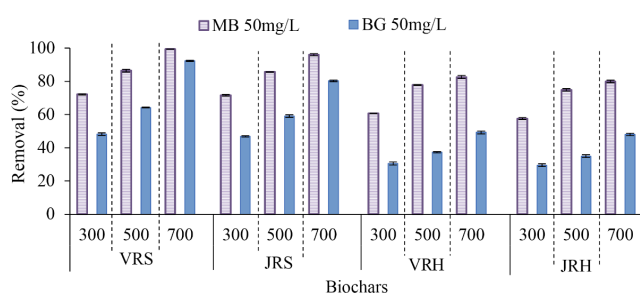


Fig. 1. Effect of pyrolysis temperature on the percent removal of MB and BG by Japanese *Koshihikari* and Vietnamese *IR50404* rice straw and rice husk produced at 300, 500 and 700°C. (Experimental conditions: T = 25°C, C₀ = 50 mg/L, m_{biochar} = 2 g/l, t = 240 min, pH ~ 7 for MB, pH ~ 2 for BG).

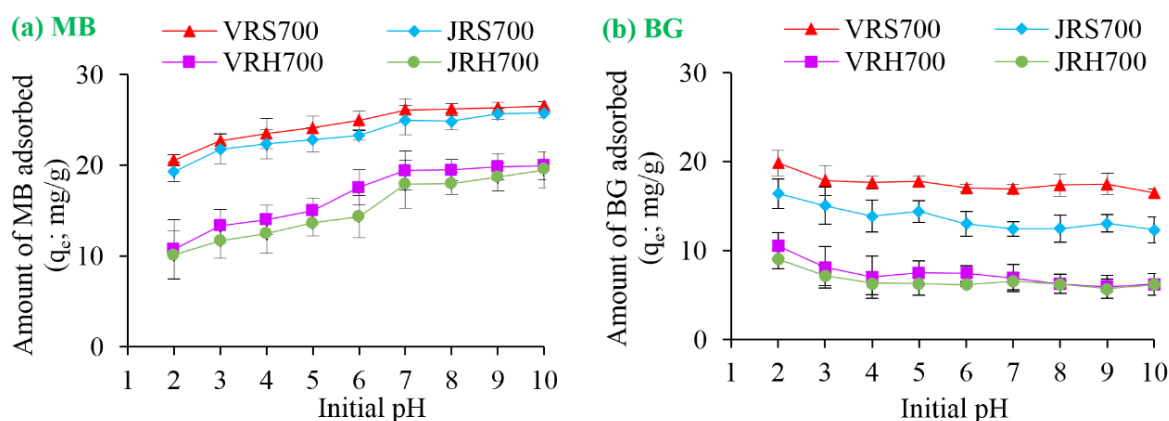


Fig. 2. Effect of pH on adsorption capacity of (a) MB and (b) BG (Experimental conditions: T = 25°C, C₀ = 50 mg/L, m_{biochar} = 2 g/l, t = 240 min, pH = 2–10).

the higher surface area of biochars produced at 700°C was believed to provide more adsorption sites for dye molecules, therefore, they were chosen to investigate the adsorption isotherms and kinetics of the studied dyes.

3.5. Effect of solution pH

Fig. 2 gives the adsorption capacity of MB and BG within pH range of 2.0–10.0. The results of pH_{pzc} test show that the pH_{pzc} determined equals to 6.9 for VRS700, 6.80 for JRS700, 6.00 for VRH700 and 5.90 for JRH700 (see Supplementary Material Fig. SM1). Theoretically, below the pH_{pzc} of biochar, the surface charge of the biochar is positively charged, whereas at pH above pH_{pzc} the biochar surface becomes negative. The solution pH also affects the ionic form in which the dye molecules exist depending on its pK_a. Generally, for a cationic dye, at pH below the pK_a value, the dye is protonated and exists in its cationic form. Therefore, if the solution pH is below both the pH_{pzc} and pK_a of the biochar and the cationic dye, respectively, both the biochar surface and the cationic dye will possess net positive charges, results in electrostatic repulsion and leading to a decrease in the amount of cationic dye absorbed onto biochars. Maximum adsorption is achieved when the solution pH is above both the biochar pH_{pzc} and the ionizable dye's pK_a value, where the biochar surface and the dye molecules possess opposite charges.

Therefore, the uptake of MB increased with the increase in the solution pH and the maximum uptake of MB was observed at pH 7.0 (up to 91–95% for rice straw biochars and 67–70% for rice husk biochars). This is consistent with others, where MB adsorption capacities are significantly improved at a higher solution pH [17,18]. This can be explained by the electrostatic attraction between the positively charged MB⁺ (solution pH > pK_a, MB) and the negatively charged surface of biochar (solution pH > pH_{pzc}). Increasing solution pH increases the number of carboxylate anion (–COO[–]) and hydroxyl (–OH) groups on the surface of biochars, thus, increases the number of negatively charged sites [44]. In this study, the electrostatic attraction between the oxygenated surface functional groups (i.e., –OH and –COOH) of biochars and N⁺ of MB may govern the adsorption pro-

cess. In addition, these functional groups would be less protonated under high solution pH [45]. Thus, attraction of MB^+ was enhanced. At low pH values, the poor adsorption of MB could be due to the competition of MB^+ with the H^+ and H_3O^+ ions for the adsorption sites on biochars. Moreover, many protons will be available to protonate the biochar surface in the condition; thereby the electrostatic repulsion between positively charged MB^+ and positively charged adsorption sites causes the decrease in the MB dye adsorption [46]. The adsorption capacity of biochars for MB dye at low pH values probably due to the other interactions such as hydrogen bonding, porous diffusion, π - π or π^+ - π interaction. In addition, biochar surface is always negative at very low pH due to a considerable excess in the number of negatively charged groups compared to positively charged groups [47–49]. This is in agreement with Tian et al. [45]. The authors claimed that at $\text{pH} < \text{pH}_{\text{pzc}}$, the weak physical forces such as hydrogen bonding, van der Waals' interactions and the chemisorption might be involved in the adsorption process [45]. Electrostatic interaction between dye ions and biochar surface was the main mechanism responsible for the removal of MB on biochars produced from various biochars, including vermicompost [50], cattle manure [51], and sewage sludge [52].

Since the surface of the biochars is strongly negatively-charged at the solution pH above both the biochar pH_{pzc} and the ionizable dye's pK_a value, the electrostatic repulsion occurred between the negatively-charged dye BG molecule and the surface of the biochar, resulting the lower amount of anionic dye to be adsorbed by biochars, with around 74–76% for rice straw biochars and only 23–26% for rice husk biochars. In brief, the maximum value of MB dye removal appeared when the $\text{pH} \geq 7$, whereas BG appeared when the $\text{pH} < 3$. However, an increasing pH solution from 7 to 10, the amount of MB adsorbed just slightly increased. As a result, for all subsequent studies, $\text{pH} \sim 7$ and $\text{pH} \sim 2$ were selected for cationic and anionic dye experiments, respectively.

3.6. Effect of biochar dosage

Absorbent dosage is a significant impact factor of adsorption process, determining the adsorbent-adsorbate equilibrium of the system [53]. In order to determine

the effect of adsorbent dose on removal percentage of MB and BG dyes, amount of biochar dose was varied within a range of 1–5 g/L keeping the dye concentration constant at 100 mg/L. Effect of biochar dose on removal percentage of MB and BG is shown in Fig. 3. It is observed that the percentage of dye adsorption increased with an increase in biochar dosage (see the solid lines with vertical axis of the left side figure), but, at the same time, the amount of dye adsorbed decreased generally (the dashed lines with vertical axis of the right side figure).

In the case of VRS700, for example, the adsorption percentage of MB and BG increased as the dosage increases from 1–5 g/L, and then maintained at approximately 100% for MB and 82% for BG until the biochar dosage reaches to 5g/L. However, the adsorption capacity of MB and BG did not perform similar to the adsorption percentage, declining gradually from 75.78 to 19.69 mg/g for MB dye, from 61.12 to 17.33 mg/g for BG dye. It also could be found that significant effects on the MB and BG adsorption exist as biochar dosage was lower than 2 g/L. When the dosage was 2 g/L, the amount MB adsorbed by VRS700 was 49.63 mg/g while the adsorption efficiency was 98.69%; and the amount BG adsorbed was 38.43 mg/g while the adsorption efficiency was 74.7%. However, the adsorption efficiency did not change significantly with further increasing dosage (i.e., when the dosage is higher than 2 g/L). Similar trends were observed in cases of JRS700, but at the slightly lower adsorbed values. For rice husk biochars, the amount adsorbed per unit mass also decreased, but there was only a little difference between VRH700 and JRH700, and their adsorbed values were much lower than VRS700. Thus, to save the amount of biochar and make full use of the adsorption capability of VRS700, JRS700, VRH700 and JRH700; 2.0 g/L biochar was selected as the optimum dose.

Overall, it is evident that the adsorption capacities of both MB and BG decreased while the adsorption percentage increased with an increase in the dosage of biochars in the 1–5 g/L range. A similar trend was shown in previous studies for MB adsorption with biochar prepared from vermicompost [50] or Eucalyptus bark [26]. To explain, with an increase in the biochar dosage, the number of available adsorption sites increases, leading to the percent removal of MB and BG increases. However, the high biochar dosage can attribute to particle interactions, for example, aggrega-

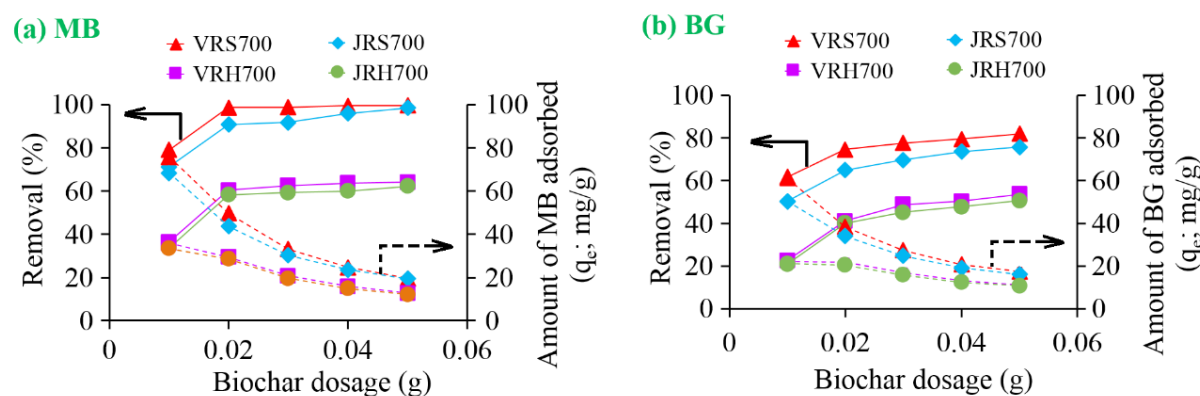


Fig. 3. Effect of biochar dosage on percent removal (%) and adsorption capacity (q_e , mg/g) of (a) MB and (b) BG. (Experimental conditions: $T = 25^\circ\text{C}$, $C_0 = 100 \text{ mg/L}$, $m_{\text{biochar}} = 1\text{--}5 \text{ g/L}$, $t = 240 \text{ min}$, $\text{pH} \sim 7$ for MB, $\text{pH} \sim 2$ for BG).

tion of adsorption sites [54]. Such aggregation might result in a decrease in total biochar surface area available to the dyes and an increase in diffusion path length [55]. As a result, the amount of dye (mg) absorbed per gram of biochar decreases with increasing biochar dosage.

3.7. Effect of contact time and adsorption kinetics

The effect of contact time (1–720 min) on the q_t values at 25°C is shown in Fig. 4. It may be seen that the MB and BG dyes were rapidly adsorbed in the first 1–20 min, the adsorption rate then decreased gradually and reached equilibrium in about 240 min. To explain, at the beginning, the uptake rate for dyes is very high as many available adsorption sites for dye molecules. As the sites are gradually filled up, adsorption becomes slow due to dye aggregation at the surface. This aggregation causes difficulties for dye molecules to diffuse deeper into the biochar pores [56]. The percentage removal at 720 min contact time was found to be higher by a maximum of ~3% than those obtained after 240

min contact time. For this reason, the optimum contact time was chosen as 240 min for adsorption.

The plots of nonlinear forms of the three kinetic models, the pseudo-second-order, Elovich and intra-particle diffusion are shown in Fig. 4. Their nonlinear kinetic parameters are tabulated in Table SM4 (Supplementary Material). As can be seen from the Table SM4, the χ^2 values in pseudo-second-order kinetic model were smallest, and its regression coefficient R^2 values were highest. Moreover, the calculated equilibrium adsorption capacities ($q_{e,cal}$) of Pseudo-second-order were in close agreement with the experimental values ($q_{e,exp}$). These results suggest that the adsorption data was well presented by pseudo-second-order kinetic, implying that the adsorption process was controlled by chemical interaction, possibly via electrostatic attraction as confirmed previously in the effect of solution pH.

The intra-particle diffusion model was used to identify the diffusion mechanism. In Fig. 5, the plots of q_t versus $t^{1/2}$ for the intra-particle diffusion models of MB and BG adsorption onto biochars showed three similar interdepen-

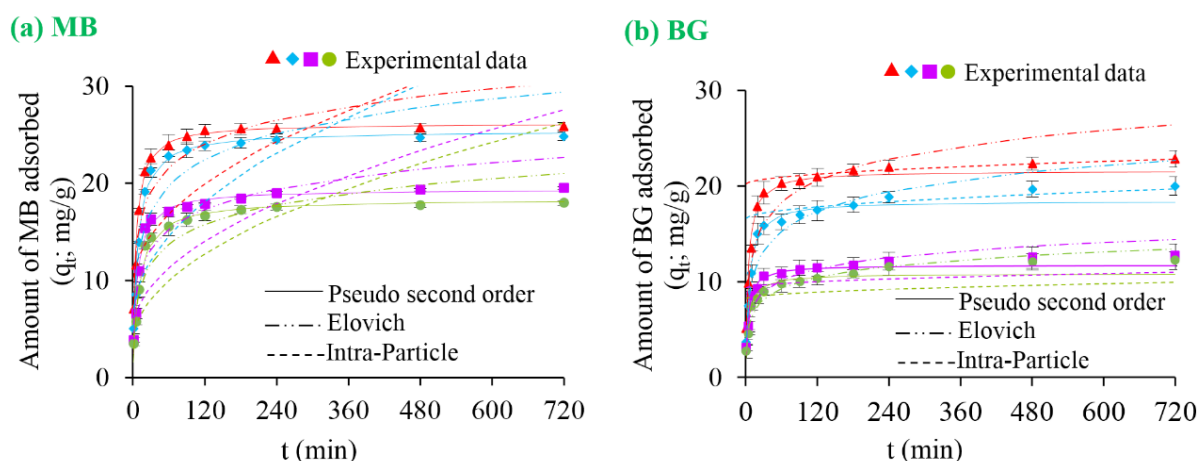


Fig. 4. Effect of contact time and nonlinear fitting of the pseudo-second-order, Elovich & intra-particle diffusion kinetic models for (a) MB and (b) BG adsorption (Symbols for experimental data: ▲VRS700; ◆JRS700; ■VRH700; ●JRH700). (Experimental conditions: $T = 25^\circ\text{C}$, $C_0 = 50 \text{ mg/L}$, $m_{\text{biochar}} = 2 \text{ g/l}$, $t = 1\text{--}720 \text{ min}$, $\text{pH} \sim 7$ for MB, $\text{pH} \sim 2$ for BG).

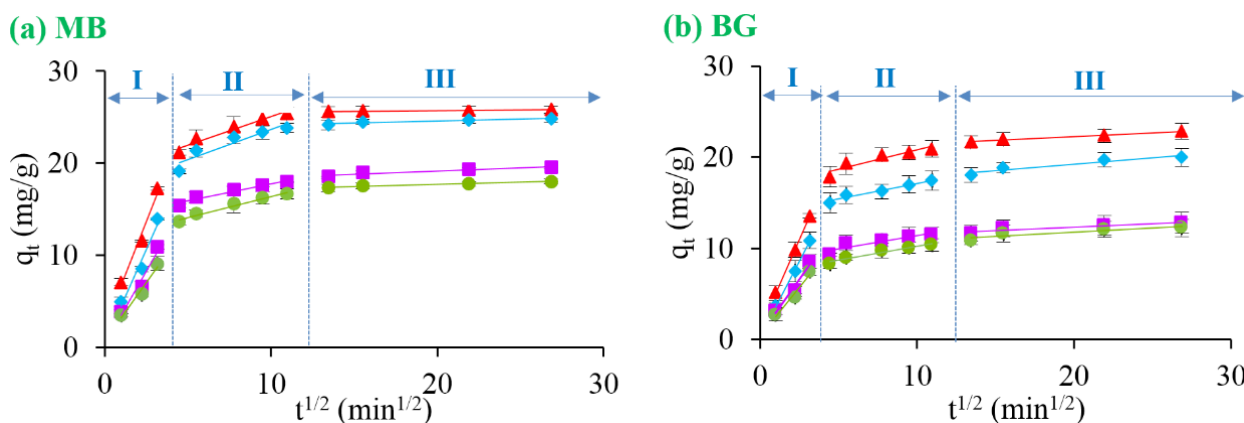


Fig. 5. Intra-particle diffusion plots of the linear form for (a) MB and (b) BG adsorption (Symbols for experimental data: ▲VRS700; ◆JRS700; ■VRH700; ●JRH700). (Experimental conditions: $T = 25^\circ\text{C}$, $C_0 = 50 \text{ mg/L}$, $m_{\text{biochar}} = 2 \text{ g/l}$, $t = 1\text{--}720 \text{ min}$, $\text{pH} \sim 7$ for MB, $\text{pH} \sim 2$ for BG).

dent linear lines, indicating that there were three stages take place during adsorption process [57]. In the first sharper linear stage (stage I: $t = 1\text{--}10$ min), external diffusion or liquid film diffusion occurred, and the dye uptake was quite rapid. This stage involved the transport of dye molecules from the bulk liquid phase to the external surface of biochars through a liquid boundary layer. This was followed by an intermediate stage (stage II: $t = 20\text{--}120$ min) that showed a slower uptake, which was due to intra-particle pore diffusion of dye molecules from the exterior of the biochars into macropores, mesopores and micropores of biochars. Until the final plateau was reached (stage III: $t > 120$ min) due to adsorption equilibrium. In the third stage or the final equilibrium stage, the intra-particle diffusion started to slow down due to low dye concentration in solution phase as well as less available biochar adsorption sites. The parameters and correlation coefficients obtained for each stage are provided in Table 2. The results showed that the regression curves were straight lines with relative high correlation coefficient values ($R^2 = 0.81\text{--}0.99$), implying that porous diffusion mechanism would have a significant effect on the dye-biochar adsorption process. The calculated values of C_1 , C_2 , C_3 were all non-zero which confirmed that diffusion into the biochar pores was not the only rate-controlling step. Therefore, the dye-biochar adsorption proceeded via a complex mechanism consisting of both surface adsorption and intra-particle transport within the pores of biochars.

3.8. Effects of initial dye concentration and adsorption isotherms

Various initial dye concentration, varied from 10 to 200 mg/L, was evaluated and is presented in Fig. 6. With increasing in the initial dye concentration from 10 to 50 mg/L, the amount of the dye adsorbed per unit mass biochars (q_e) rapidly increased, due to the high number of unoccupied adsorption sites on the biochar surface offered a greater chance for dye adsorption. When the dye concentration in solution was increased from 80 to 200 mg/L, the adsorption sites available in the biochars became more quickly saturated, thereby reducing the efficiency of dye adsorption capacity.

The nonlinear fitting of Langmuir, Freundlich, and Temkin isotherms is also presented in Fig. 6, and their

parameters are summarized in Table SM5 (Supplementary Material). The χ^2 values for Langmuir model were smallest, together with the highest R^2 values obtained, also, the calculated data from this model was quite similar to the experimental data. These results confirmed that Langmuir model appropriately described the isotherms of the dye adsorption process, indicating monolayer adsorption.

The theoretical monolayer maximum adsorption capacities (q_m) for MB calculated from the nonlinear Langmuir equation at 25°C were ordered as follow: VRS700 (67.69 mg/g) > JRS700 (56.88 mg/g) > VRH700 (33.28 mg/g) > JRH700 (32.81 mg/g). The adsorption of anionic BG dye followed the same order of cationic MB dye; however, the Langmuir adsorption capacity values were much lower than for cationic MB dye (Table SM5 Supplementary Material). These results further confirm that biochars from Vietnamese IR50404 showed higher dye adsorption capacity than Japanese Koshihikari variety and were significantly more effective for cationic MB dye, as already found in the effect of pyrolysis temperature. Notably, the adsorption capacity of rice straw biochars (VRS700 and JRS700) to MB and BG almost doubled rice husk biochars (VRH700 and JRH700). Reduced adsorption in rice husk biochars (VRH700 and JRH700) was probably due to the less available adsorption sites, as indicated by lower BET surface area confirmed previously.

The dimensionless constant separation factor (R_L) values obtained from Langmuir equation were between 0.04 and 0.92, together with the nonlinearity index ($1/n$) from Freundlich equation was between 0.36 and 0.53 at 25°C (data not shown), indicating the favourability of the dye adsorption onto biochars under studied conditions. Therefore, the selected biochars were suitable adsorbents for MB and BG from aqueous solution.

The results of MB adsorption kinetics and isotherm somewhat agreed with other rice-waste-residue-derived chars. For example, the adsorption kinetics of MB dye by rice hull ash well-fitted with the pseudo-second-order model while the adsorption isotherms fitted the Langmuir isotherm, with the maximum adsorption capacities (q_m) values of greater than 45 mg/g [58]. In another study, the sorption of MB on organosolv lignin extracted from rice straw also shows that the pseudo-second order model fitted best

Table 2
Intra-particle diffusion kinetic parameters for MB, SO, MO and BG adsorption, calculated by the linearization technique

Dye	Biochar	Intra-particle diffusion (linearized form)								
		Stage I: $t = 1\text{--}10$ min			Stage II: $t = 20\text{--}120$ min			Stage III: $t > 120$ min		
		C_1	k_{p1}	R^2	C_2	k_{p2}	R^2	C_3	k_{p3}	R^2
MB	VRS700	2.04	4.64	0.98	18.82	0.62	0.96	25.34	0.02	0.99
	JRS700	0.45	4.07	0.96	17.05	0.66	0.88	23.65	0.05	0.88
	VRH700	0.29	3.20	0.96	14.03	0.37	0.95	17.74	0.07	0.86
	JRH700	0.64	2.56	0.96	11.83	0.46	0.97	16.71	0.05	0.95
BG	VRS700	1.15	3.91	0.99	16.54	0.42	0.87	20.60	0.08	0.98
	JRS700	0.31	3.30	0.99	13.65	0.35	0.96	16.46	0.14	0.91
	VRH700	0.41	2.47	0.97	8.48	0.29	0.81	10.76	0.08	0.91
	JRH700	0.41	2.14	0.96	7.12	0.31	0.93	9.91	0.09	0.81

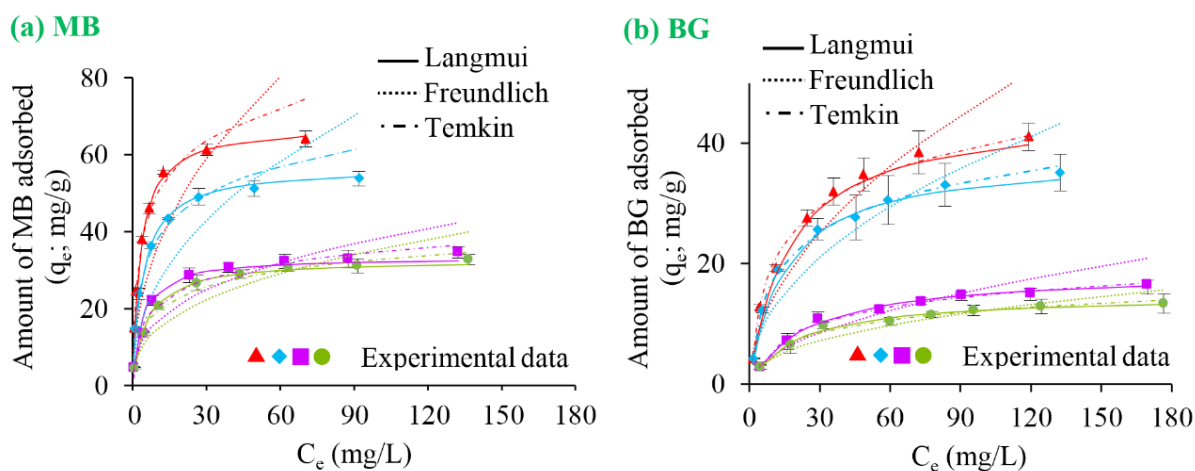


Fig. 6. Effect of initial dye concentration and nonlinear fitting of Langmuir, Freundlich and Temkin isotherm models for (a) MB, (b) SO, (c) MO and (d) BG adsorption (Symbols for experimental data: ▲VRS700; ◆JRS700; ◆VRH700; ●JRH700). (Experimental conditions: $T = 25^{\circ}\text{C}$, $C_0 = 10\text{--}200\text{ mg/L}$, $m_{\text{biochar}} = 2\text{ g/l}$, $t = 240\text{ min}$, $\text{pH} \sim 7$ for SO, $\text{pH} \sim 2$ for BG).

the kinetic data, while the Langmuir model described very well the adsorption isotherm, with the q_m of 40.02 mg/g [36]. For activated carbon produced from rice husk, the results of adsorption kinetics of MB show that the rates of sorption were found to conform to pseudo-second-order and intra-particle diffusion kinetics; whereas, adsorption isotherm followed Langmuir–Hinshelwood model, and the q_m value was 301.18 mg/g [34]. To remove Bromocresol Green from water solutions, Shokrollahi et al. (2011) used a species of *Ziziphus* native, namely *Ziziphus nummularia*. Adsorption kinetic data could be interpreted by both pseudo second-order and intraparticle diffusion models; while the isothermal data was in line with the Temkin, Freundlich, and Langmuir adsorption isotherms, with the adsorption capacity of 6.21 mg/g [30].

3.9. Effect of temperature and adsorption thermodynamics

A temperature range of $25\text{--}45^{\circ}\text{C}$ ($298\text{--}318\text{K}$) was used to evaluate the effect of temperature on dye adsorption. As illustrated in Figs. SM2 and SM3 Supplementary Material, the amount of MB and BG adsorbed on biochars increased slightly with increasing temperature, indicating the endothermic nature of the ongoing adsorption. To explain, increasing temperature may produce swelling effects within the internal structure of the biochar, which enables dye molecules penetrate further into smaller pores of biochars. Also, as the temperature increases, the rate of diffusion of the dye molecules across the external boundary layer and into the internal pores of the biochar particles may be increased, resulting in higher adsorption capacities of biochars [59].

The nonlinear Langmuir plots for the adsorption of MB and BG onto biochars at temperatures 25 , 35 and 45°C are also presented in Figs. SM2 and SM3, respectively. Since the adsorption isotherm data fitted well to the Langmuir model, K_L constant obtained from nonlinear optimization technique was used to calculate thermodynamic parameters ΔG° , ΔH° and ΔS° . As shown in Table SM6 Supplementary Material, the negative ΔG° values were obtained ($\Delta G^{\circ} =$

$35.27\text{--}41.94\text{ kJ/mol}$), indicating that the adsorption process of cationic and anionic dyes was both thermodynamically favorable and spontaneous under experimental conditions [60]. It could be observed that when the temperature increased from 298 to 318 K , the ΔG° values decreased by 7.3 to 10.9% for MB, and 7.6 to 9.7% for BG adsorption. This denotes the increase in spontaneity of all adsorption systems, leading to the higher removal efficiency of these dyes at higher temperatures. The positive values for ΔH° indicates the endothermic nature of the adsorption process. Physisorption, such as van der Waals interactions, is usually lower than 20 kJ/mol , and electrostatic interaction ranges from 20 to 80 kJ/mol . Chemisorption bond strengths can be from 80 to 450 kJ/mol [61]. In this study, the low ΔH° values obtained for all dye adsorption ($\Delta H^{\circ} = 3.92\text{--}23.69\text{ kJ/mol}$), implying that physical interaction and also electrostatic interaction would have a significant effect on the adsorption rate. The ΔS° was also positive, corresponding to an increased randomness on the biochar surface during the uptake of dye molecules. In conclusion, values of ΔG° and ΔH° confirm the spontaneous and endothermic nature of the adsorption process, which was consistent with the results of several studies [62,63].

3.10. Possible adsorption mechanism

The low enthalpy values obtained from thermodynamic study is an indication that physisorption was probably the main mechanism of adsorption for both anionic dye and cationic dye. Physical adsorption mechanism may occur via porous diffusion, hydrogen bonding, $\pi\text{--}\pi$ interaction and $\pi^+\text{--}\pi$ interaction between the dye molecules and biochars [16,64,65]. These physical mechanisms are proposed in Fig. 7.

3.10.1. Porous diffusion

The porous diffusion mechanism of MB and BG dye molecules was suggested to consist of two distinct adsorp-

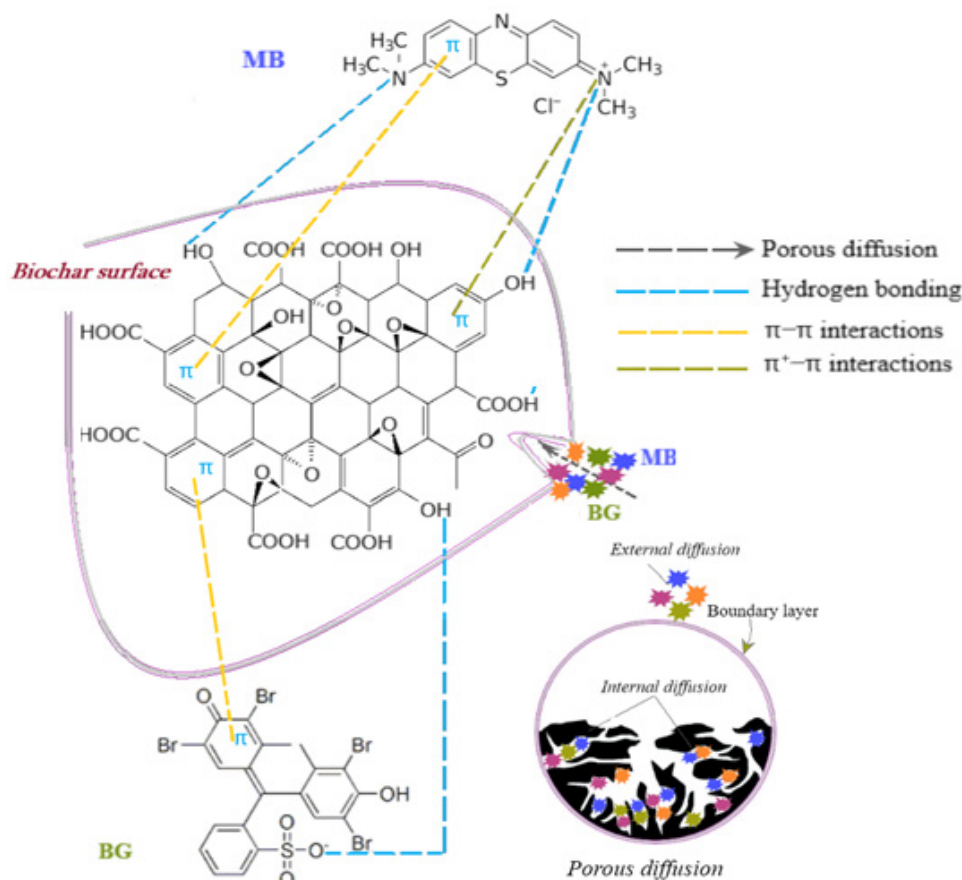


Fig. 7. Possible physical adsorption mechanism of MB and BG onto biochar surface.

tion steps. The first step may be the external diffusion of the dye molecules from the boundary layer to the surface of the biochar. This may follow by the internal diffusion in which the penetration of the dye molecules into the pores of the biochar occurs.

3.10.2. Hydrogen bonding

Generally, hydrogen bonding is favoured on material with oxygen-containing groups as in the case of the biochar material. Hydrogen bonding interaction may occur between the H-bonds (i.e., $-\text{COOH}$ or $-\text{OH}$ which act as the H-donors) on the biochar surface and the nitrogen or oxygen atoms in dyes (i.e., nitrogen atoms in the MB molecules, or the oxygen atoms in the BG molecules, which act as the H-acceptors).

3.10.3. π - π interaction and π^+ - π interaction

π - π interaction is a noncovalent interaction between π -acceptor and π -donor molecules, while π^+ - π interaction (or cation- π interaction) is a noncovalent interaction between a surface of an aromatic π -donor and a cation. In π - π interaction, the aromatic rings in biochar may act as π -electron donors and the aromatic rings in MB and BG dyes may act as π -electron acceptors. Also, molecular structures of MB possess a cation N^+ , which may lead to the binding of cation

N^+ to the π -face of aromatic rings in biochar surface, forming π^+ - π interaction.

The experimental results of pH effects show that adsorption of cationic MB dye was favoured as pH increases. However, the adsorption of anionic BG dye was not favoured at high pH values because the electrostatic repulsion and the presence of OH^- ions in excess competing with the dye anions for the adsorption sites. Therefore, besides physical interaction as found, another major mode of adsorption of cationic dyes could be chemisorption. Chemical adsorption mechanism of MB on biochars may likely be due to an electrostatic attraction between the oxygenated surface functional groups (i.e., $-\text{OH}$ and $-\text{COOH}$) of biochars and N^+ of MB molecules [50,66]. This electrostatic attraction is illustrated in Fig. 8.

3.11. Comparison with other adsorbents

The adsorption capacities of rice straw and rice husk derived biochars into MB and BG dyes have been compared with other agriculture solid waste biochar, biomass activated carbon and other materials as presented in Table 3. Compared to other adsorbents and activated carbons for BG removal, the adsorption capacities of studied biochars were not larger. But bi—nts for the BG removal from aqueous solutions.

For MB dye adsorption, also from Table 3, it shows that rice straw and rice husk biochars studied in this work

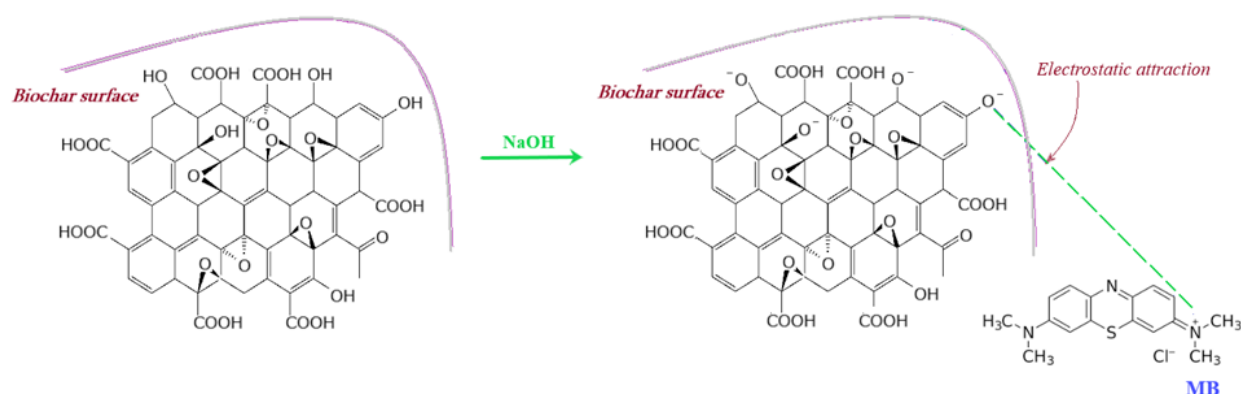


Fig. 8. Possible chemical adsorption mechanism via electrostatic attraction of MB onto biochar surface.

Table 3

Comparison of the maximum adsorption capacity (q_m value) for MB and BG of rice straw and rice husk derived biochars with those of other adsorbents

Adsorbate	Adsorbent	Adsorption capacity (mg/g)	Contact time (min)	Ref.
BG	<i>Ziziphus nummularia</i>	6.21	8	[30]
	Cotton stalks activated carbon	222.22	180	[23]
	<i>Phragmites karka</i> activated carbon	392.3	300	[31]
	poly(2-phenoxy ethyl [bis(2-hydroxy ethyl)amino]acetate)	52.63	90	[32]
	Rice straw biochar	37.79–45.47	240	This study
	Rice husk biochar	14.78–18.08	240	This study
MB	poly(2-phenoxy ethyl [bis(2-hydroxy ethyl)amino]acetate)	31.25	90	[32]
	Kenaf fibre biochar	18.18	1440	[25]
	Rabbit faeces biochar	86.85	210	[27]
	Pig manure biochar	46.96	210	[27]
	Cotton stalks activated carbon	153.85	180	[23]
	Peanut shell activated carbon	208.33	1440	[21]
	<i>F. infectoria</i> activated carbon	151.6	20	[22]
	Rice husk activated carbon	343.50	120	[24]
	Rice straw activated carbon	472.10	120	[24]
	Raw rice husk	17	360	[28]
	NaOH-rice husk	39.2	360	[28]
	Ultrasound assisted -rice husk	23.5	360	[28]
	Supercritical CO ₂ -rice husk	18.4	360	[28]
	Modified rice straw	296.74	60	[29]
	Organosolv lignin from rice straw	40	120	[36]
	Rice straw biochar	56.88–67.69	240	This study
	Rice husk biochar	32.81–33.28	240	This study

have a comparative adsorption capacity to MB compared to some biomass biochars and raw materials. In comparison to activated carbon, however, the adsorption capacity of MB was smaller. This result can be predicted because activated carbon generally possesses a higher degree of porosity which has been developed during manufacture at high temperature. In addition, it has a large surface area owning much more sites for dye molecules. Briefly, rice straw and rice husk biochars obtained are likely suitable and promising adsorbents for MB removal from

aqueous solutions since they have relatively high adsorption capacities.

4. Conclusions

This paper reports the experimental results of the adsorption of two dyes, Methylene Blue and Bromocresol Green, over the adsorbent biochars. This is the first paper to study the adsorption capacity of these dyes

by biochars from Japan and Vietnam rice varieties. Biochars were produced from rice straw and rice husk of two rice varieties, Japanese *Koshihikari* and Vietnamese *IR50404*. Within pH adjusted from 2 to 10, cationic MB dye favored at $\text{pH} \geq 7$, whereas $\text{pH} < 3$ preferred for anionic BG dye adsorption. The adsorption isotherm data fitted well to the Langmuir model. The adsorption capacity of cationic MB dye on the biochars was significantly more effective than anionic BG dye adsorption. Biochars from Vietnamese *IR50404* obtained the higher adsorption efficiency compared to Japanese *Koshihikari* variety, which attributed to the higher surface area in their biochars. Intraparticle diffusion affected the adsorption rates of the adsorption systems. While the anionic dye adsorption process was mainly controlled by physisorption, the cationic dye adsorption was simultaneously controlled by both physical and chemical interactions. Physical adsorption mechanism may occur via hydrogen bonding between the H-bonds of $-\text{OH}$ (or $-\text{COOH}$) of biochars and nitrogen atom of the MB molecules (or the oxygen atom in the BG molecules), π - π interaction between the aromatic rings of biochars and the aromatic rings of MB and BG dyes, or π^+ - π interaction between cation N^+ of the dye molecules and aromatic rings of biochars. Chemisorption occurred via electrostatic attraction between the oxygenated surface functional groups (i.e., $-\text{OH}$ and $-\text{COOH}$) of biochars and N^+ of MB may govern the cationic adsorption process.

This study confirmed that the biochar adsorbents prepared from rice straw and rice husk - low cost agricultural wastes - could selectively remove MB and BG from an aqueous solution. By using biochars produced from these available wastes as economically and cheap friendly adsorbents, a certain amount of undesired MB and BG, even though other colors/dyes from industrial effluents can be achieved. Therefore, it can be substituting other expensive adsorbents, such as activated carbon. With the experimental data obtained in this study, it is possible to design and optimize an economical treatment process for the dye removal from industrial effluents by biochars produced from rice residues. And thus, the two benefits can be obtained simultaneously, including removing the rice wastes and treating unwanted coloured effluents.

Acknowledgment

The authors would like to acknowledge The Ministry of Education, Culture, Sports, Science and Technology of Japan (MEXT) for research funding.

References

- [1] J. Ndi Nsami, J. Ketcha Mbadcam, The adsorption efficiency of chemically prepared activated carbon from cola nut shells by on methylene blue, *J. Chem.*, 2013 (2013).
- [2] M. Verma, N. M'hamdi, Z. Dkhili, S.K. Brar, K. Misra, In: Bio-transformation of Waste Biomass into High Value Biochemicals, Thermochemical Transformation of Agro-biomass into Biochar: Simultaneous Carbon Sequestration and Soil Amendment, Springer, 2014, pp. 51–70.
- [3] R.L. Singh, Principles and Applications of Environmental Biotechnology for a Sustainable Future, Springer, 2017.
- [4] M. Ejder-Korucu, A. Gürses, Ç. Doğar, S.K. Sharma, M. Açıkyıldız, Removal of organic dyes from industrial effluents: an overview of physical and biotechnological applications, *Green Chemistry for Dyes Removal from Wastewater: Research Trends and Applications*, (2015) 1–34.
- [5] Ö. Aktas, F. Çeçen, In: Activated carbon for water and wastewater treatment: Integration of adsorption and biological treatment, *Fundamentals of Adsorption onto Activated Carbon in Water and Wastewater Treatment*, John Wiley & Sons, 2011.
- [6] B. Kasprzyk-Hordern, Chemistry of alumina, reactions in aqueous solution and its application in water treatment, *Adv. Colloid Interface Sci.*, 110 (2004) 19–48.
- [7] N. Koshy, D. Singh, Fly ash zeolites for water treatment applications, *J. Environ. Chem. Eng.*, 4 (2016) 1460–1472.
- [8] A.A. Adeyemo, I.O. Adeoye, O.S. Bello, Adsorption of dyes using different types of clay: a review, *Appl. Water. Sci.*, 7 (2017) 543–568.
- [9] C. Santhosh, V. Velmurugan, G. Jacob, S.K. Jeong, A.N. Grace, A. Bhatnagar, Role of nanomaterials in water treatment applications: a review, *Chem. Eng. J.*, 306 (2016) 1116–1137.
- [10] A.C. Sophia, T. Arfin, E.C. Lima, Recent Developments in Adsorption of Dyes Using Graphene Based Nanomaterials, In: *A New Generation Material Graphene: Applications in Water Technology*, Springer, 2019, pp. 439–471.
- [11] D. Mehta, S. Mazumdar, S. Singh, Magnetic adsorbents for the treatment of water/wastewater—a review, *J. Water Process Eng.*, 7 (2015) 244–265.
- [12] A. Bonilla-Petriciolet, D.I. Mendoza-Castillo, H.E. Reynel-Ávila, Adsorption processes for water treatment and purification, Springer, 2017.
- [13] C. Peiris, S.R. Gunatilake, J.J. Wewalwewa, M. Vithanage, In: *Biochar from Biomass and Waste: Fundamentals and Applications*, Biochar and biochar composites: low cost adsorbents for environmental remediation, Elsevier, 2018.
- [14] M.B. Ahmed, J.L. Zhou, H.H. Ngo, W. Guo, Adsorptive removal of antibiotics from water and wastewater: progress and challenges, *Sci. Total Environ.*, 532 (2015) 112–126.
- [15] N. Hagemann, K. Spokas, H.-P. Schmidt, R. Kägi, M. Böhler, T. Bucheli, Activated carbon, biochar and charcoal: linkages and synergies across pyrogenic carbon's ABCs, *Water*, 10 (2018) 182.
- [16] V.O. Shikuku, W.N. Nyairo, C.O. Kowenje, In: *Advanced Treatment Techniques for Industrial Wastewater*, Preparation and Application of Biochars for Organic and Microbial Control in Wastewater Treatment Regimes, IGI Global, 2019, pp. 19–34.
- [17] P. Hadi, S.K. Sharma, G. McKay, In: *Green Chemistry for Dyes Removal from Wastewater: Research Trends and Applications*, Removal of Dyes from Effluents Using Biowaste-Derived Adsorbents, Scrivener Publishing LLC, 2015, pp. 139–201.
- [18] X. Xiao, B. Chen, In: *Agricultural and Environmental Applications of Biochar: Advances and Barriers Interaction mechanisms between biochar and organic pollutants*, Soil Science Society of America, 2016, pp. 225–258.
- [19] Z. Abbas, S. Ali, M. Rizwan, I.E. Zaheer, A. Malik, M.A. Riaz, M.R. Shahid, M.Z. ur Rehman, M.I. Al-Wabel, A critical review of mechanisms involved in the adsorption of organic and inorganic contaminants through biochar, *Arabian J. Geosci.*, 11 (2018) 448.
- [20] O.D. Nartey, B. Zhao, Biochar preparation, characterization, and adsorptive capacity and its effect on bioavailability of contaminants: an overview, *Adv. Mater. Sci. Eng.*, 2014 (2014).
- [21] X. Han, L. Chu, S. Liu, T. Chen, C. Ding, J. Yan, L. Cui, G. Quan, Removal of methylene blue from aqueous solution using porous biochar obtained by KOH activation of peanut shell biochar, *BioResources*, 10 (2015) 2836–2849.
- [22] S. Ravulapalli, R. Kunta, Effective removal of methylene blue, a hazardous dye from industrial effluents using active carbon of *F. infectoria* plant, *Int. J. Environ. Sci. Technol.*, (2018) 1–12.
- [23] M. Özdemir, Ö. Durmuş, Ö. Şahin, C. Saka, Removal of methylene blue, methyl violet, rhodamine B, alizarin red, and bromocresol green dyes from aqueous solutions on activated cotton stalks, *Desal. Water Treat.*, 57 (2016) 18038–18048.

- [24] N. Kannan, M.M. Sundaram, Kinetics and mechanism of removal of methylene blue by adsorption on various carbons—a comparative study, *Dyes Pigment.*, 51 (2001) 25–40.
- [25] D.K. Mahmoud, M.A.M. Salleh, W.A.W.A. Karim, A. Idris, Z.Z. Abidin, Batch adsorption of basic dye using acid treated kenaf fibre char: equilibrium, kinetic and thermodynamic studies, *Chem. Eng. J.*, 181 (2012) 449–457.
- [26] S. Dawood, T.K. Sen, C. Phan, Adsorption removal of Methylene Blue (MB) dye from aqueous solution by bio-char prepared from Eucalyptus sheathiana bark: kinetic, equilibrium, mechanism, thermodynamic and process design, *Desal. Water Treat.*, 57 (2016) 28964–28980.
- [27] W. Huang, J. Chen, J. Zhang, Adsorption characteristics of methylene blue by biochar prepared using sheep, rabbit and pig manure, *Environ. Sci. Pollut. Res.*, 25 (2018) 29256–29266.
- [28] D.S. Franco, E.H. Tanabe, D.A. Bertuol, G.S. dos Reis, É.C. Lima, G.L. Dotto, Alternative treatments to improve the potential of rice husk as adsorbent for methylene blue, *Water Sci. Technol.*, 75 (2017) 296–305.
- [29] A. Ebrahimian Pirbazari, B. Fakhari Kisom, M. Ghamangiz Khararoodi, Anionic surfactant-modified rice straw for removal of methylene blue from aqueous solution, *Desal. Water Treat.*, 57 (2016) 18202–18216.
- [30] A. Shokrollahi, A. Alizadeh, Z. Malekhosseini, M. Ranjbar, Removal of bromocresol green from aqueous solution via adsorption on ziziphus nummularia as a new, natural, and low-cost adsorbent: Kinetic and thermodynamic study of removal process, *J. Chem. Eng. Data*, 56 (2011) 3738–3746.
- [31] B. Murmu, S. Behera, S. Das, R. Mohapatra, B. Bindhani, P. Parhi, Extensive investigation on the study for the adsorption of Bromocresol Green (BCG) dye using activated *Phragmites karka*, *NISCAIR-CSIR*, 25 (2018) 409–420.
- [32] G. Torğut, K. Demirelli, Comparative adsorption of different dyes from aqueous solutions onto polymer prepared by ROP: kinetic, equilibrium and thermodynamic studies, *Arab. J. Sci. Eng.*, 43 (2018) 3503–3514.
- [33] R. Sun, Cereal Straw as a Resource for Sustainable Biomaterials and Biofuels: Chemistry, Extractives, Lignins, Hemicelluloses and Cellulose, Elsevier, 2010.
- [34] M. Ahiduzzaman, A.S. Islam, Preparation of porous bio-char and activated carbon from rice husk by leaching ash and chemical activation, *SpringerPlus*, 5 (2016) 1248.
- [35] T.J. Kindala, S.J. Kayembe, K.A. Kifuani, L.B. Ilinga, K.M. Taba, Removal of methylene blue, bromocresol green and methyl red dyes from aqueous solutions by adsorption using *Bryophyllum pinnatum* (Lam.) kurz stem powder and its activated carbon, *Congo Sciences*, 3 (2015).
- [36] S. Zhang, Z. Wang, Y. Zhang, H. Pan, L. Tao, Adsorption of methylene blue on organosolv lignin from rice straw, *Procedia Environ. Sci.*, 31 (2016) 3–11.
- [37] P.T. Do, T. Ueda, R. Kose, L.X. Nguyen, T. Okayama, T. Miyaniishi, Properties and potential use of biochars from residues of two rice varieties, Japanese *Koshihikari* and Vietnamese *IR50404*, *J. Mater. Cycles Waste Manage.*, 21 (2019) 98–106.
- [38] M. Uchimiya, S. Chang, K.T. Klasson, Screening biochars for heavy metal retention in soil: role of oxygen functional groups, *J. Hazard. Mater.*, 190 (2011) 432–441.
- [39] Y. Yang, Y. Chun, G. Sheng, M. Huang, pH-dependence of pesticide adsorption by wheat-residue-derived black carbon, *Langmuir*, 20 (2004) 6736–6741.
- [40] J.J. Pignatello, S. Kwon, Y. Lu, Effect of natural organic substances on the surface and adsorptive properties of environmental black carbon (char): attenuation of surface activity by humic and fulvic acids, *Environ. Sci. Technol.*, 40 (2006) 7757–7763.
- [41] F. Hao, X. Zhao, W. Ouyang, C. Lin, S. Chen, Y. Shan, X. Lai, Molecular structure of corn-cob-derived biochars and the mechanism of atrazine sorption, *Agron. J.*, 105 (2013) 773–782.
- [42] G.N. Kasozi, A.R. Zimmerman, P. Nkedi-Kizza, B. Gao, Catechol and humic acid sorption onto a range of laboratory-produced black carbons (biochars), *Environ. Sci. Technol.*, 44 (2010) 6189–6195.
- [43] C.E. Brewer, Biochar characterization and engineering, Iowa State University (2012).
- [44] W. Zhang, H. Yan, H. Li, Z. Jiang, L. Dong, X. Kan, H. Yang, A. Li, R. Cheng, Removal of dyes from aqueous solutions by straw based adsorbents: batch and column studies, *Chem. Eng. J.*, 168 (2011) 1120–1127.
- [45] Y. Tian, C. Ji, M. Zhao, M. Xu, Y. Zhang, R. Wang, Preparation and characterization of baker's yeast modified by nano-Fe₃O₄: Application of biosorption of methyl violet in aqueous solution, *Chem. Eng. J.*, 165 (2010) 474–481.
- [46] A.E. Pirbazari, E. Saberikhah, S.H. Kozani, Fe₃O₄-wheat straw: preparation, characterization and its application for methylene blue adsorption, *Water Resour. Ind.*, 7 (2014) 23–37.
- [47] L. Beesley, E. Moreno-Jiménez, J.L. Gomez-Eyles, E. Harris, B. Robinson, T. Sizmur, A review of biochars' potential role in the remediation, revegetation and restoration of contaminated soils, *Environ. Pollut.*, 159 (2011) 3269–3282.
- [48] J. Lehmann, M.C. Rillig, J. Thies, C.A. Masiello, W.C. Hockaday, D. Crowley, Biochar effects on soil biota – A review, *Soil Biol. Biochem.*, 43 (2011) 1812–1836.
- [49] A. Mukherjee, A. Zimmerman, W. Harris, Surface chemistry variations among a series of laboratory-produced biochars, *Geoderma*, 163 (2011) 247–255.
- [50] G. Yang, L. Wu, Q. Xian, F. Shen, J. Wu, Y. Zhang, Removal of congo red and methylene blue from aqueous solutions by vermicompost-derived biochars, *PloS One*, 11 (2016) e0154562.
- [51] Y. Zhu, B. Yi, Q. Yuan, Y. Wu, M. Wang, S. Yan, Removal of methylene blue from aqueous solution by cattle manure-derived low temperature biochar, *RSC Adv.*, 8 (2018) 19917–19929.
- [52] T. Chen, B. Yan, D.-M. Xu, L.-I. Li, Enhanced adsorption performance of methylene blue from aqueous solutions onto modified adsorbents prepared from sewage sludge, *Water Sci. Technol.*, 78 (2018) 803–813.
- [53] H. Devenci, Y. Kar, Adsorption of hexavalent chromium from aqueous solutions by bio-chars obtained during biomass pyrolysis, *J. Ind. Eng. Chem.*, (2013) 190–196.
- [54] T. Chen, Z. Zhou, R. Han, R. Meng, H. Wang, W. Lu, Adsorption of cadmium by biochar derived from municipal sewage sludge: impact factors and adsorption mechanism, *Chemosphere*, 134 (2015) 286–293.
- [55] G.L. Dotto, S.K. Sharma, L.A. Pinto, In: *Green Chemistry for Dyes Removal from Wastewater: Research Trends and Applications*, Biosorption of organic dyes: Research opportunities and challenges, Scrivener Publishing LLC, 2015, pp. 295–329.
- [56] R. Kumar, R. Ahmad, Biosorption of hazardous crystal violet dye from aqueous solution onto treated ginger waste (TGW), *Desalination*, 265 (2011) 112–118.
- [57] S. Figaro, J. Avril, F. Brouers, A. Ouensanga, S. Gaspard, Adsorption studies of molasse's wastewaters on activated carbon: Modelling with a new fractal kinetic equation and evaluation of kinetic models, *J. Hazard. Mater.*, 161 (2009) 649–656.
- [58] X.-G. Chen, S.-S. Lv, S.-T. Liu, P.-P. Zhang, A.-B. Zhang, J. Sun, Y. Ye, Adsorption of methylene blue by rice hull ash, *Sep. Sci. Technol.*, 47 (2012) 147–156.
- [59] M. Doğan, M. Alkan, A. Türkyilmaz, Y. Özdemir, Kinetics and mechanism of removal of methylene blue by adsorption onto perlite, *J. Hazard. Mater.*, 109 (2004) 141–148.
- [60] J. Mellis EV, Soares MR, da Cruz MCP, de Camargo OA, In: *Competitive sorption and transport of heavy metals in soils and geological media, Sorption of Heavy Metals in Tropical Soils*, CRC Press, 2012.
- [61] J.S. Piccin, T.R.S.A. Cadaval, L.A.A. de Pinto, G.L. Dotto, In: *Adsorption Processes for Water Treatment and Purification*, Adsorption isotherms in liquid phase: experimental, modeling, and interpretations, Springer, 2017, pp. 19–51.
- [62] D.A.G. Sumalinog, S.C. Capareda, M.D.G. de Luna, Evaluation of the effectiveness and mechanisms of acetaminophen and methylene blue dye adsorption on activated biochar derived from municipal solid wastes, *J. Environ. Manage.*, 210 (2018) 255–262.

- [63] L. Sun, D. Chen, S. Wan, Z. Yu, Performance, kinetics, and equilibrium of methylene blue adsorption on biochar derived from eucalyptus saw dust modified with citric, tartaric, and acetic acids, *Bioresour. Technol.*, 198 (2015) 300–308.
- [64] Y. Tong, P. McNamara, B.K. Mayer, Adsorption of organic micropollutants onto biochar: A review of relevant kinetics, mechanisms and equilibrium, *Environ. Sci.: Water Res. Technol.*, 5 (2019) 821–838.
- [65] H. Lyu, Y. Gong, R. Gurav, J. Tang, In: *Biochar Application: Essential soil microbial ecology*, Potential application of biochar for bioremediation of contaminated systems, Elsevier, 2016.
- [66] H.N. Tran, S.-J. You, T.V. Nguyen, H.-P. Chao, Insight into the adsorption mechanism of cationic dye onto biosorbents derived from agricultural wastes, *Chem. Eng. Comm.*, 204 (2017) 1020–1036.

Supplementary material

Supplementary methods

Adsorption kinetics and modelling

Adsorption kinetic experiments were carried out in a 15 mL conical centrifuge tubes containing 10 mL dye solution with initial concentrations of 50 mg/L and biochar dose of 2 g/L. pH of 7 was chosen for cationic dyes (MB and SO), while pH of 2 was controlled to anionic dyes (MO and BG). The temperature and adsorption time were 25°C and 240 min, respectively. Sample tubes were shaken on a shaker (Bioshaker BR-23FH) and operated at 200 rpm. The samples were prepared to be easily withdrawn at various time intervals (1, 10, 20, 30, 60, 90, 120, 180, 240, 480 and 720 min). The suspension was centrifuged at 3000 rpm for 10 min and then were filtered through the Whatman filter paper. The filtrates were measured by UV-visible Recording spectrophotometer (Shimadzu UV-2100), at maximum absorbance of the dyes (see Table 1). To obtain the absorbance-concentration profiles of the dyes, calibration curve was plotted between absorbance and concentration of the dye. Three different kinetic models, i.e., pseudo-second order, Elovich and intraparticle diffusion model were used. Their non-linearized (functional form) and linearized equations are included in Table SM1 below.

Pseudo-second order model assumes that the rate-limiting step in adsorption may be chemisorption and the adsorption capacity is proportional to the number of active sites on adsorbent. The Elovich equation assumes that the solid surfaces are heterogeneous and therefore, exhibit different activation energies for chemisorption. Unlike the Pseudo-second order and Elovich kinetic models, intraparticle diffusion model explains the adsorption progress of the adsorbate intraparticle of the adsorbent. According to this model, if intra-particle diffusion is only the controlling

mechanism on overall adsorption process, q_t versus $t^{1/2}$ plot will give a straight-line plot passes through the origin point. In contrast, the line which does not pass through the original point implies that intraparticle diffusion is not the only mechanism. If the data present multilinear plots, then two or more steps are included in the sorption process such as external diffusion and intraparticle diffusion.

Adsorption isotherms and modelling

Adsorption isotherms were determined by shaking 0.02 g samples of biochar with a 10-ml dye solution, using concentrations from 10 to 200 mg/L, and the other conditions were the same as the kinetic experiment. The non-linear and linear forms of three well-known isothermal models, namely Langmuir, Freundlich and Temkin, were applied to explain adsorption equilibrium. Their nonlinearized and linearized equations are included in Table SM2.

The Langmuir is valid for monolayer adsorption on a surface with a finite number of adsorption sites of equal energy, while the Freundlich isotherm derives by assuming a heterogeneous surface with a nonuniform distribution of heat of adsorption over the surface. Unlike the Langmuir isotherm, the Temkin isotherm considers the interaction between the adsorbate molecules already adsorbed and to be adsorbed. In this isotherm, the heat of sorption of all the molecules in the layer would decrease linearly with coverage due to adsorbate/adsorbent interactions. It makes the Temkin model differ from Freundlich model which implies a logarithmical decrease in the heat of adsorption.

Based on the Langmuir equation, a dimensionless constant separation factor R_L can be used to predict whether adsorption system is favorable or not. R_L is calculated by using the following equation:

$$R_L = \frac{1}{1 + K_L C_0}$$

Table SM1
Adsorption kinetic models

Kinetic	Functional form	Linear form	Plot	Parameters and constants
Pseudo-second order	$\frac{dq_t}{dt} = k_2(q_e - q_t)^2$	$\frac{t}{q_t} = \frac{1}{k_2 q_e^2} + \frac{1}{q_e} t$	$\log t/q_t$ versus t	q_e : Equilibrium adsorption capacity (mg/g); q_t : Time adsorption capacity (mg/g); t : the contact time (min); k_2 : Second-order rate coefficient (g/mg·min)
Elovich equation	$\frac{dq_t}{dt} = \alpha \exp(-\beta q_t)$	$q_t = \frac{1}{\beta} \ln(\alpha\beta) + \frac{1}{\beta} \ln t$	q_t versus $\ln t$	q_t : Time adsorption capacity (mg/g) t : the contact time (min); α : initial adsorption rate (mg/g·min); β : related to the extended of surface coverage and activation energy for chemisorption (g/mg).
Intraparticle diffusion	$q_t = k_p t^{1/2} + C$	$q_t = k_p t^{1/2} + C$	q_t versus $t^{1/2}$	q_t : Time adsorption capacity (mg/g) k_p : the intra-particle diffusion rate constant (mg/g·min ^{1/2}); t : the contact time (min); C : the constant related to the thickness of the boundary layer (mg/g).

Table SM2
Adsorption isotherm models

Isotherm	Functional form	Linear form	Plot	Parameters and constants
Langmuir	$q_e = \frac{q_m K_L C_e}{1 + K_L C_e}$	$\frac{C_e}{q_e} = \frac{1}{K_L q_m} + \frac{C_e}{q_m}$	$\frac{C_e}{q_e}$ versus C_e	q_e : Adsorption capacity (mg/g); q_m : The maximum adsorption capacity (mg/g); C_e : Equilibrium concentration of the adsorbate (mg/l); K_L : the Langmuir adsorption constant (L/mg).
Freundlich	$q_e = K_F C_e^{1/n}$	$\log q_e = \log K_F + (1/n) \log C_e$	$\log q_e$ versus $\log C_e$	q_e : Adsorption capacity (mg/g); C_e : Equilibrium concentration of the adsorbate (mg/l); K_F : The sorption affinity, (mg/kg)/(mg/L) ⁿ ; $1/n$: The nonlinearity index (unitless).
Temkin	$q_e = \frac{RT}{b} \ln(K_T C_e)$	$q_e = \frac{RT}{b} \ln K_T + \frac{RT}{b} \ln C_e$	q_e versus $\ln C_e$	q_e : Adsorption capacity (mg/g); C_e : Equilibrium concentration of the adsorbate (mg/l); K_T : Equilibrium association constant (l/mg); b : Variation of the adsorption energy (J/mol) R : Gas constant (8.314 J/mol.K); T : The absolute temperature in Kelvin (273 + °C).

Table SM3
Basic physical and chemical characteristics of the biochar samples

Feedstock	VRS			JRS			VRH			JRH		
	300	500	700	300	500	700	300	500	700	300	500	700
Pyrolysis Temperature (°C)												
<i>Ultimate analysis^a</i>												
C (%)	49.68	50.65	46.91	52.30	54.00	51.27	40.61	41.89	43.28	42.92	38.42	37.97
H (%)	1.22	0.65	0.19	1.89	0.99	0.28	1.01	0.78	0.29	1.19	0.56	0.38
N (%)	0.90	0.80	0.48	1.47	0.48	0.31	0.61	0.51	0.48	1.76	0.46	0.34
O ^b (%)	13.54	11.54	14.18	9.09	6.97	7.90	15.48	13.80	10.03	11.79	11.67	11.44
H/C atomic ratio	0.29	0.15	0.05	0.43	0.22	0.07	0.30	0.22	0.08	0.33	0.17	0.12
O/C atomic ratio	0.20	0.17	0.23	0.13	0.10	0.12	0.29	0.25	0.17	0.21	0.23	0.23
<i>Proximate analysis^a</i>												
Moisture (%)	3.70	2.61	1.95	3.98	3.25	2.12	3.85	2.98	2.08	4.07	3.32	2.12
Volatile (%)	25.38	15.45	8.91	28.79	17.62	9.50	27.46	17.86	10.63	27.54	18.58	10.95
Total ash (%)	30.98	33.76	36.31	31.29	34.32	38.13	38.45	40.05	43.86	38.28	45.58	47.77
<i>Pore characteristics</i>												
S _{BET} (m ² /g)	51.58	131.37	377.99	23.45	127.78	293.00	25.89	147.13	245.05	19.50	105.28	235.69
S _{external} (m ² /g)	6.06	23.42	85.59	6.74	18.10	53.15	5.62	40.13	85.54	0.12	7.83	48.47
S _{micropore} (m ² /g)	45.51	107.95	292.40	16.72	109.69	239.86	20.28	107.00	159.51	19.38	97.45	187.22
V _{total} (cm ³ /g)	0.064	0.111	0.299	0.051	0.171	0.171	0.045	0.107	0.188	0.033	0.070	0.164
V _{micropore} (cm ³ /g)	0.020	0.048	0.13	0.007	0.048	0.106	0.009	0.047	0.070	0.008	0.043	0.082
V _{non-micro} (cm ³ /g)	0.044	0.063	0.17	0.043	0.123	0.065	0.036	0.060	0.118	0.025	0.027	0.082
Average pore size (nm)	4.98	3.38	3.16	8.66	5.37	2.33	6.89	2.92	3.06	6.79	2.74	2.80

^aValues are the average of triplicates

^bData are calculated by difference

where C_0 is the initial dye concentration (mg/L).

The value of R_L indicates the shape of Langmuir isotherm to be either unfavourable ($R_L > 1$), linear ($R_L = 1$), irreversible ($R_L = 0$), or favourable ($0 < R_L < 1$). A smaller R_L value indicates a highly favourable adsorption.

Based on the Freundlich equation, the value of n also indicates a favorable adsorption when $1 < n < 10$ and it is more favorable as $1/n < 1$, while $1/n$ equal to 1 indicates linear adsorption leading to identical adsorption energies for all sites.

Table SM4

Pseudo-second-order, Elovich and intraparticle diffusion kinetic parameters for MB and BG adsorption by VRS700, JRS700, VRH700 and JRH700, calculated by the nonlinearization optimization technique (Experimental conditions: $T = 25^{\circ}\text{C}$, $C_0 = 50 \text{ mg/L}$, $m_{\text{biochar}} = 2 \text{ g/l}$, $t = 1\text{--}720 \text{ min}$, $\text{pH} \sim 7$ for MB, $\text{pH} \sim 2$ for BG)

Dye	Biochar	Pseudo-second order					Elovich				Intra-particle diffusion			
		$q_{e,\text{exp}}$	$q_{e,\text{cal}}$	k_2	χ^2	R^2	β	α	χ^2	R^2	C	k_p	χ^2	R^2
		mg/g	mg/g	g/mg·min			g/mg	mg/g·min			mg/g	mg/g·min ^{1/2}		
MB	VRS700	24.59	26.19	0.008	0.02	0.99	0.28	25.64	3.26	0.83	9.37	0.96	21.73	0.08
	JRS700	23.84	25.39	0.005	0.11	0.98	0.26	10.04	4.20	0.84	6.00	1.10	30.32	0.05
	VRH700	22.06	19.40	0.007	0.15	0.96	0.33	7.94	3.04	0.85	4.66	0.85	22.36	0.09
	JRH700	20.64	18.37	0.005	0.29	0.95	0.34	5.08	2.90	0.86	3.36	0.85	22.92	0.05
BG	VRS700	19.25	21.62	0.011	0.85	0.97	0.30	14.23	2.58	0.91	20.13	0.10	19.62	-0.15
	JRS700	18.93	18.45	0.010	0.92	0.96	0.33	8.10	1.97	0.90	16.51	0.12	17.88	-0.05
	VRH700	10.84	11.77	0.022	0.67	0.95	0.58	9.96	1.17	0.88	9.33	0.06	7.79	0.23
	JRH700	9.70	10.85	0.020	1.04	0.92	0.60	7.01	0.62	0.95	8.22	0.06	8.33	0.25

Table SM5

Langmuir, Freundlich, and Temkin isotherms parameters for MB and BG adsorption by VRS700, JRS700, VRH700 and JRH700, calculated by the nonlinearization optimization technique (Experimental conditions: $T=25^{\circ}\text{C}$, $C_0 = 10\text{--}200 \text{ mg/L}$, $m_{\text{biochar}} = 2 \text{ g/l}$, $t = 240 \text{ min}$, $\text{pH} \sim 7$ for MB, $\text{pH} \sim 2$ for BG)

Dye	Biochar	Langmuir				Freundlich				Temkin			
		q_m	k_L	χ^2	R^2	$1/n$	k_F	χ^2	R^2	b	k_T	χ^2	R^2
		mg/g	L/mg			(mg/kg)/(mg/L) ⁿ				J/mol	l/mg		
MB	VRS700	67.69	0.32	5.77	0.98	0.46	12.21	46.12	0.58	193.35	4.79	4.15	0.96
	JRS700	56.88	0.23	5.62	0.98	0.45	9.27	32.02	0.55	229.24	3.26	4.48	0.95
	VRH700	33.28	0.26	1.30	0.97	0.36	7.30	6.97	0.80	402.01	2.84	5.54	0.96
	JRH700	32.81	0.17	0.20	0.99	0.39	5.94	6.64	0.80	419.60	2.55	0.48	0.98
BG	VRS700	45.47	0.06	1.42	0.98	0.53	4.19	7.06	0.84	287.60	1.01	0.29	0.99
	JRS700	37.79	0.07	0.93	0.98	0.49	4.01	6.44	0.83	333.22	0.99	0.09	1.00
	VRH700	18.08	0.04	0.10	0.99	0.52	1.45	2.21	0.89	640.57	0.45	0.13	0.99
	JRH700	14.78	0.05	0.12	0.99	0.44	1.63	1.34	0.87	800.64	0.51	0.18	0.98

Adsorption thermodynamics

Finally, adsorption thermodynamic experiments were performed at temperatures 25°C , 35°C and 45°C under the same conditions used in isotherm experiment.

Thermodynamic parameters Gibbs free energy change ΔG^0 , change in enthalpy ΔH^0 , and change in entropy ΔS^0 is obtained by the following equation:

$$\Delta G^0 = -RT \ln K_C$$

In which R is the universal gas constant ($8.314 \text{ J/mol}\cdot\text{K}$) and T is the absolute temperature (K). The equilibrium constant K_C is calculated by:

$$K_C = K_L \cdot MW \cdot 1000 \cdot 55.5$$

where K_L is obtained from a Langmuir equation, MW is the molecular weight of dye (i.e. $MW_{\text{MB}} = 319.85$, $MW_{\text{SO}} = 350$, $MW_{\text{MO}} = 327.3$, $MW_{\text{BG}} = 698$).

Enthalpy ΔH^0 (J/mol) and entropy changes ΔS^0 (J/mol·K) are calculated as follow:

$$\ln K_C = \frac{\Delta S^0}{R} - \frac{\Delta H^0}{RT}$$

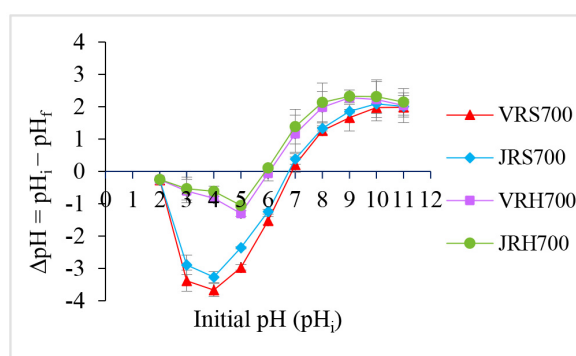


Fig. SM1. Plot for the pH_{pzc} determination of biochars.

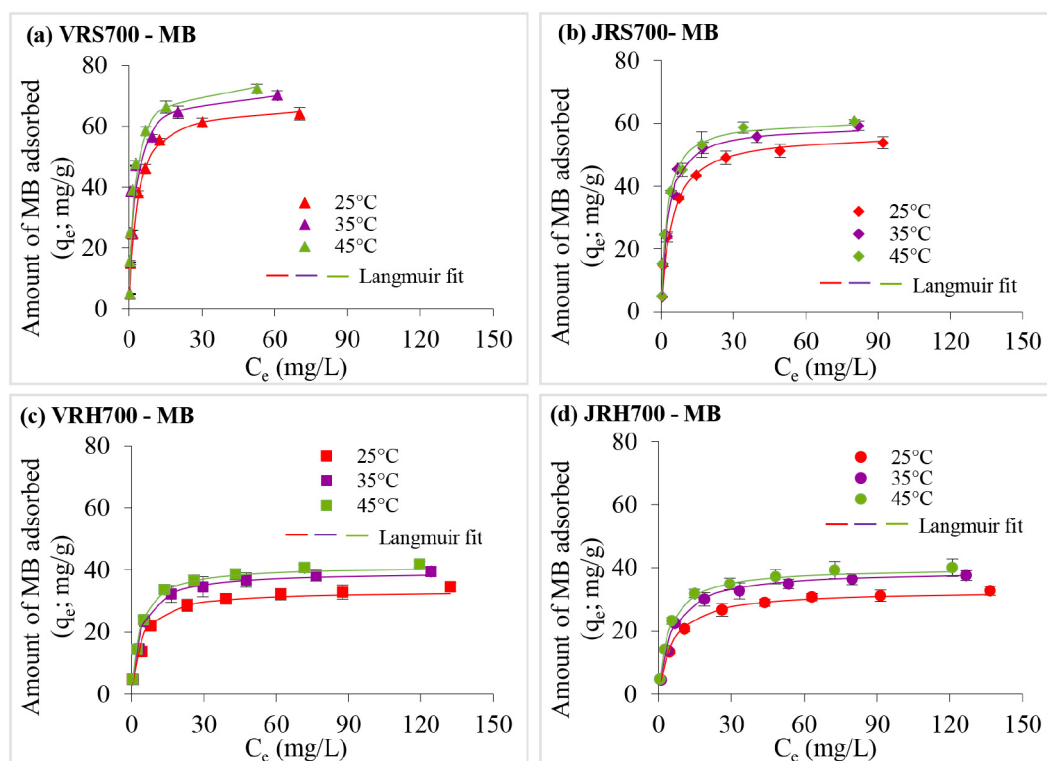


Fig. SM2. Plots of nonlinear forms of Langmuir isotherm models for MB adsorption on (a) VRS700, (b) JRS700, (c) VRH700 and (d) JRH700 at different temperatures. (Experimental conditions: $T = 25\text{--}45^\circ\text{C}$, $C_0 = 10\text{--}200$ mg/L, $m_{\text{biochar}} = 2$ g/l, $t = 240$ min, $\text{pH} \sim 7$).

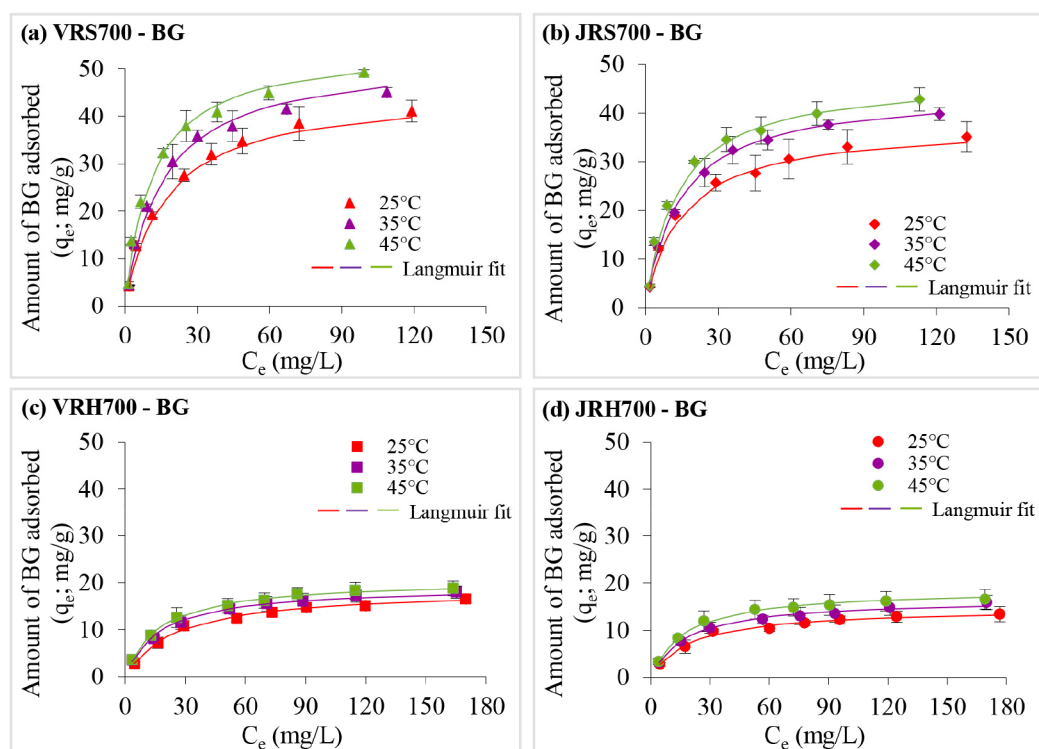


Fig. SM3. Plots of nonlinear forms of Langmuir isotherm models for BG adsorption on (a) VRS700, (b) JRS700, (c) VRH700 and (d) JRH700 at different temperatures (Experimental conditions: $T = 25\text{--}45^\circ\text{C}$, $C_0 = 10\text{--}200$ mg/L, $m_{\text{biochar}} = 2$ g/l, $t = 240$ min, $\text{pH} \sim 2$).

By plotting $\ln K_c$ versus $1/T$, ΔH^0 and ΔS^0 values can be obtained from the slope and intercept, respectively.

The negative value of ΔG^0 indicates the spontaneity of the adsorption process, and greater values (in module) reflect a more energetically favourable adsorption reaction. A positive value for ΔG^0 indicates that energy must be input, and that the reaction is nonspontaneous. Enthalpy

ΔH^0 is used to identify the nature of adsorption, in which a positive value of ΔH^0 indicates an endothermic process and negative ΔH^0 indicates the adsorption is exothermic. A positive value of ΔS^0 indicates increased randomness of adsorbate molecules on the solid surface than in solution. If ΔS^0 is positive, along with negative ΔG^0 , the adsorption is spontaneous and is reaching equilibrium.